ACCSCIENCE PUBLISHING

International Journal of Bioprinting

RESEARCH ARTICLE

Engineering a biocompatible 3D bone marrow niche model for drug screening in the *KMT2A*-rearranged acute myeloid leukaemia cell line MOLM-13

Supplementary File

(A) Supplementary methods

A1. Actin/DAPI staining

2%Alg8%Gel hand-cast and 3D-bioprinted hydrogels containing MOLM-13 cells or MOLM-13/HS5 spheroid co-culture were washed in PBS supplemented with calcium and magnesium (PBS+; Gibco), then fixed in 4% paraformaldehyde in PBS+ at 37 °C for 15 minutes. Hydrogels were washed with PBS+ and then permeabilised (10.3 g sucrose, 0.292 g sodium chloride, 0.06 g magnesium chloride (hexahydrate), 0.476 g HEPES in 100 mL PBS+, 0.5 mL Triton X-100) for five minutes at 4°C. Gels were washed with PBS+ and then blocked in 1% bovine serum albumin (BSA) for five minutes at 37°C. Gels were submerged in 1% BSA containing Alexa Fluor™ 594 Phalloidin stain (Invitrogen) and incubated for 1 hour at 37°C. After incubating, the gels were washed three times with 0.5% PBS+-Tween20 under gentle agitation. Gels were stained with VECTASHIELD Antifade mounting medium containing DAPI (Vector Laboratories, USA) prior to imaging. Images were captured at 10× and 20× magnification using the Zeiss Axiovert (hand-cast) and EVOS M7000 Imager (3D-bioprinted) (Ex/Em: Alexa Fluor™ 594 Phalloidin: 581/609 nm; DAPI: 360/460 nm).

(B) Supplementary figures and tables

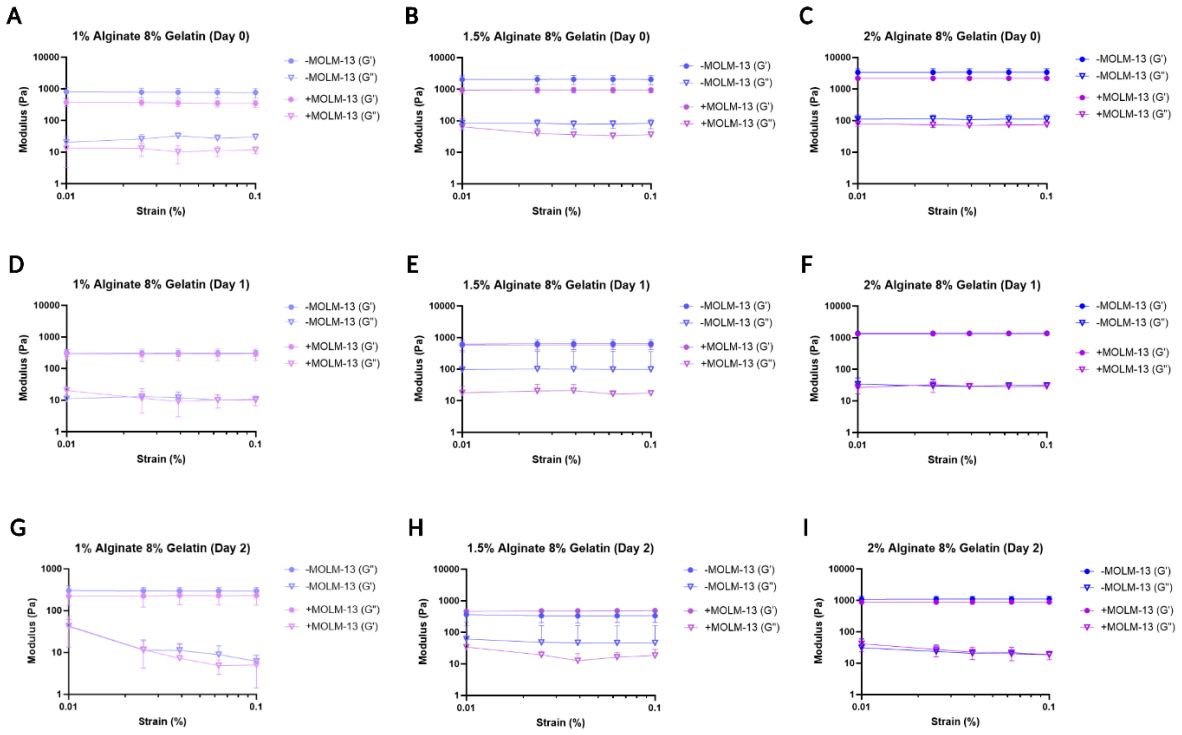

Figure S1. Strain sweeps of 1%, 1.5% and 2% Alg 8% Gel hydrogels at days 0, 1, and 2 after crosslinking. (A), (D), and (G) depict 1%Alg8%Gel at days 0, 1, and 2, respectively; (B), (E) and (H) depict 1.5%Alg8%Gel hydrogels; and (C), (F), and (I) show 2%Alg8%Gel. Closed circles show the storage modulus (G') and open triangles show the loss modulus (G"). Strain range was 0.01–0.1%, and angular frequency was 10 rad/s. Error bars depict standard deviation.

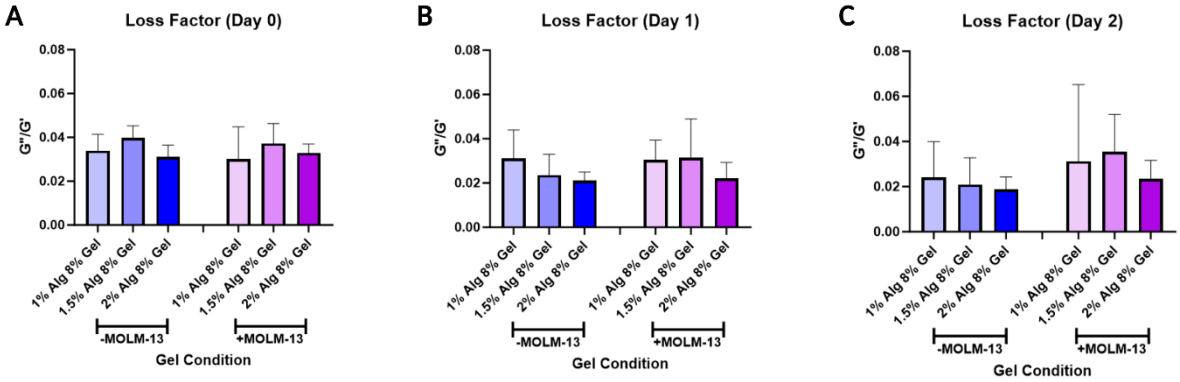

Figure S2. Loss factor of 1%, 1.5% and 2% Alg8%Gel hydrogels with and without MOLM-13 cells over two days. Loss factor was calculated as outlined in **Equation 1**. Error bars depict standard deviation.

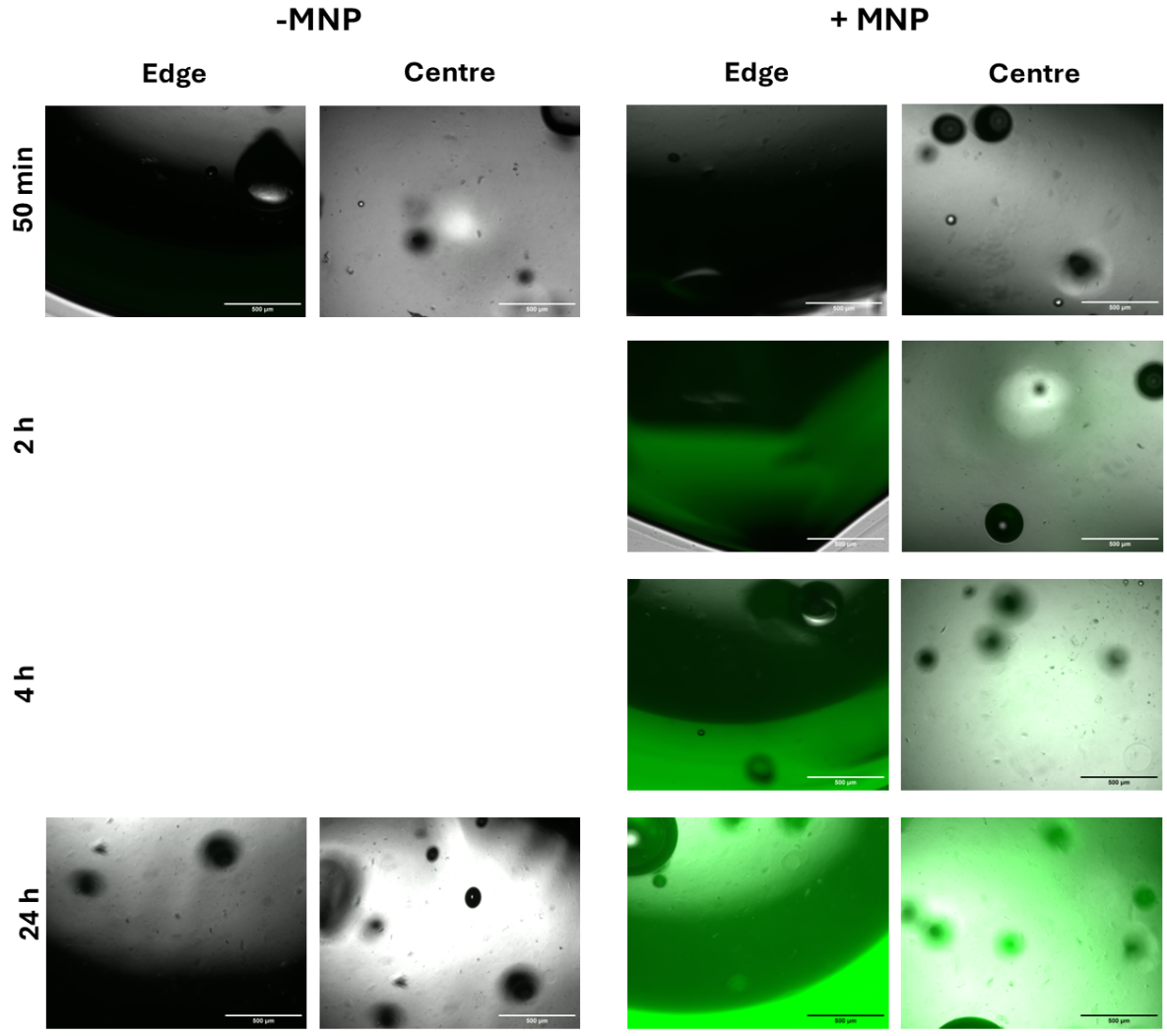

Figure S3. Diffusion of fluorescent nanoparticles through 2%Alg8%Gel hand-cast hydrogels to simulate diffusion of chemotherapeutic drugs. Hydrogels were submerged in DMEM containing FluorMag nanoparticles conjugated to FITC at 200 µg/mL and imaged at regular intervals over 24 hours. These images show that small particles can diffuse through the hydrogels after at least two hours. Images were taken using a Zeiss Axiovert microscope at 5× (scale bars: 500 µm), with the FITC channel exposure set at 800 ms across all timepoints.

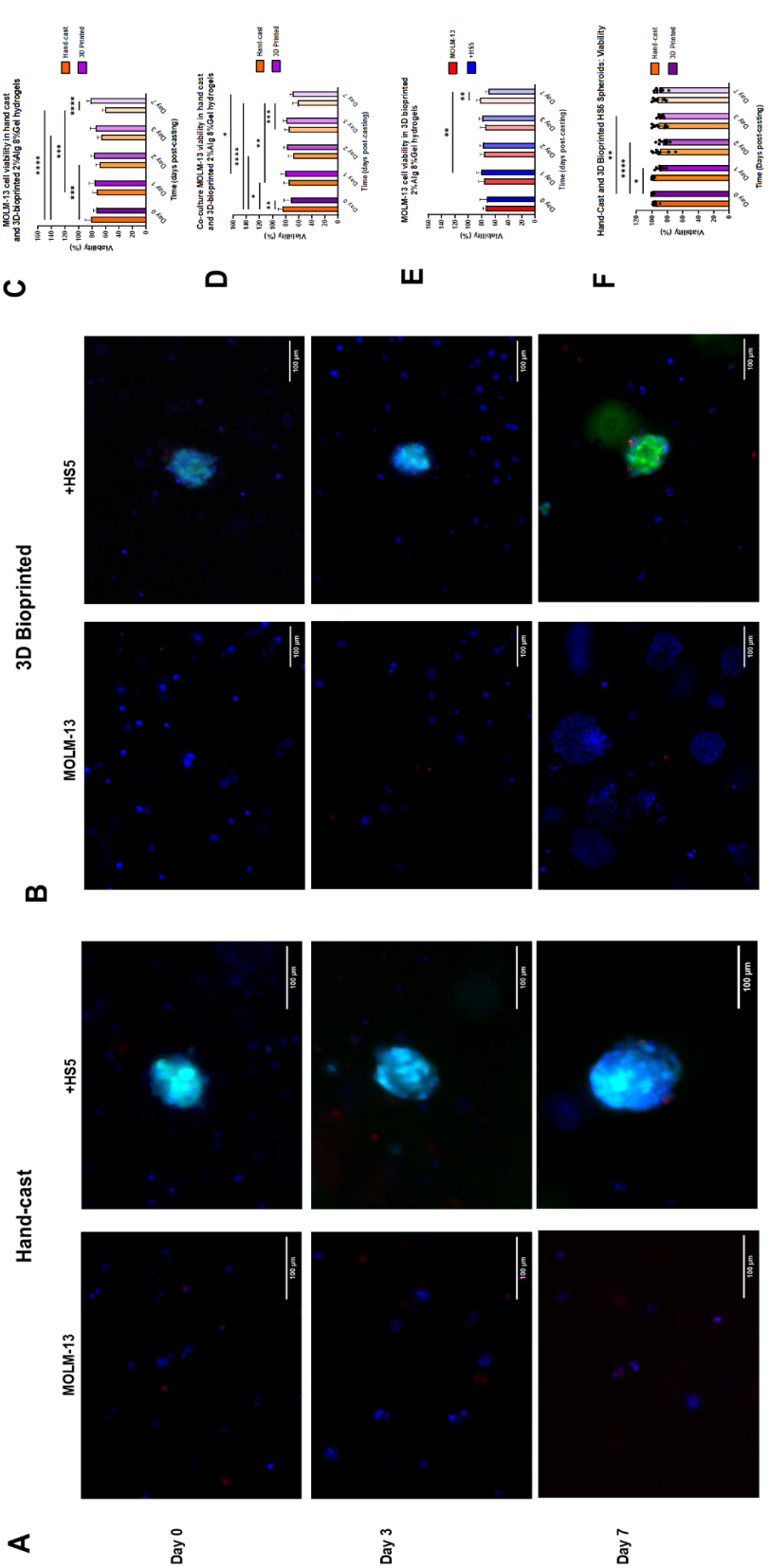

Figure S4. Viability of MOLM-13 cells and HS5 spheroids within hand-cast and 3D-bioprinted 2%Alg8%Gel hydrogels. (A) MOLM-13 cells in monoculture and co-cultured with GFP-HS5 spheroids within hand-cast 2%Alg8%Gel hydrogels stained with live/dead stain; (B) 3D-bioprinted alginate/gelatin hydrogels containing MOLM-13 cells in monoculture and co-cultured with GFP-HS5 spheroids stained with live/dead stain (20× magnification; scale bar: 100 µm); (C) Comparison of monoculture MOLM-13 viability in hand-cast and 3D-bioprinted alginate/gelatin gels; (D) Comparison of co-cultured MOLM-13 cell viability in hand-cast and 3D-bioprinted alginate/gelatin gels; (E) Comparison of MOLM-13 monoculture and HS5 co-culture viability. Green: HS5 cells (GFP-HS5 cells); blue: live cells; red: dead cells; (F) Comparison of HS5 spheroid viability in hand-cast and 3D-bioprinted hydrogels for up to seven days. HS5 spheroid viability was calculated using the JACOP plugin on Fiji, whereby Mander's coefficient was used to determine the degree of overlap of GFP (green channel) with either live (blue channel) or dead (red channel). Hand-cast viability images were taken using a Zeiss Axiovert microscope, and 3D-bioprinted viability images were taken using the EVOS M7000 Imager. Single-plane images were taken at 10× for analysis and 20× for representative images. One-way ANOVAs with multiple comparisons were used in C–F. Significance is shown using asterisks, and an absence of these indicates a lack of significance. Significance: * $p \leq 0.05$; ** $p \leq 0.01$; *** $p \leq 0.001$, **** $p \leq 0.0001$. Bars represent the average of nine technical replicates (three images per hydrogel, a total of nine data points) with standard deviation shown as error bars.

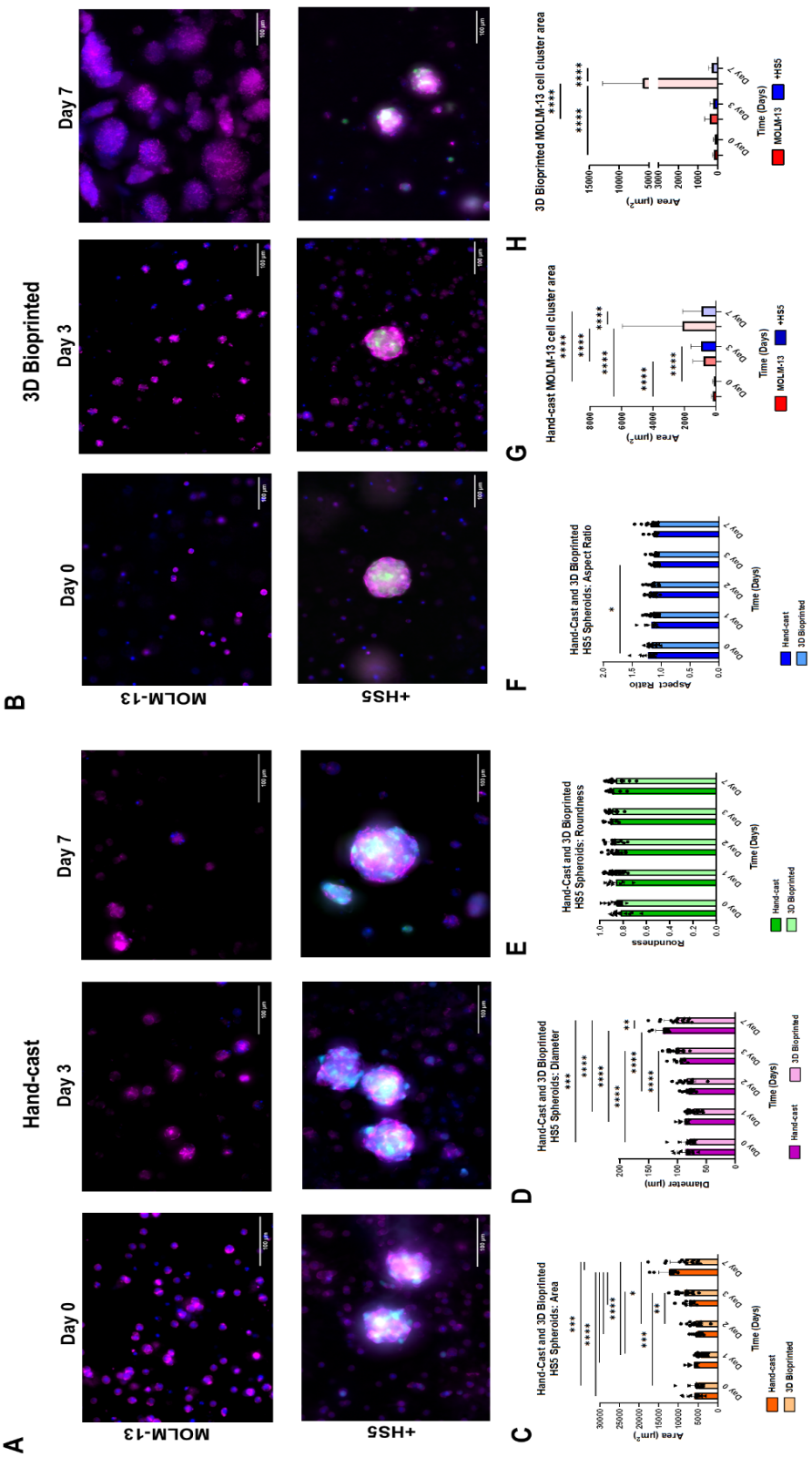

Figure S5. Morphology of MOLM-13 cells within hand-cast and 3D-bioprinted 2%Alg8%Gel hydrogels. (A) Representative images of MOLM-13 cells in monoculture and co-cultured with GFP-HS5 spheroids within hand-cast 2%Alg8%Gel hydrogels stained for F-actin and DAPI nuclear stain (20× magnification; scale bar: 100 µm); (B) MOLM-13 cells in monoculture and co-cultured with GFP-HS5 spheroids within 3D-bioprinted 2%Alg8%Gel hydrogels stained for F-actin and DAPI nuclear stain (20× magnification; scale bar: 100 µm). Green: HS5 cells; blue: DAPI (Nuclei); magenta: F-actin. Spheroids were quantified for hand-cast and 3D-bioprinted spheroids, and area (C), diameter (D), roundness (E), and aspect ratio (F) are depicted as bar charts. The cluster size of MOLM-13 cells in monoculture and HS5 co-culture in hand-cast (G) and 3D-bioprinted (H) hydrogels was quantified using Fiji and shown as bar charts. Analyses were completed using images taken at 10× magnification. Representative z-stack images were taken at 20× magnification, and the maximal intensity projection was selected to produce the final images. Hand-cast hydrogel images were taken using a Zeiss Axiovert microscope, and 3D-bioprinted images were taken using the EVOS M7000 Imager. One-way ANOVAs with multiple comparisons were used in C–H to detect significant differences between conditions. Significance is shown using asterisks, and an absence of these indicates a lack of significance. Significance: * $p \leq 0.05$; ** $p \leq 0.01$; *** $p \leq 0.001$, **** $p \leq 0.0001$. Bars represent the average of nine technical replicates (three images per hydrogel, a total of nine data points) with standard deviation shown as error bars.

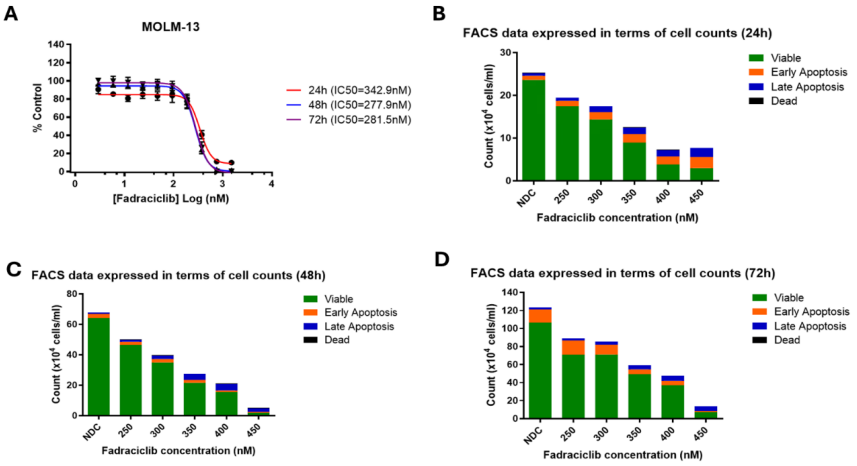

Figure S6. Determining the EC50 of fadraciclib (FAD) on MOLM-13 cells. The cells were treated with fadraciclib in a range of 250–450 nM and analysed after 24, 48, and 72 hours. (A) Logarithmic graph depicting the results of the resazurin reduction assays (n = 3) at 24 (red), 48 (blue), and 72 hours (purple). Error bars depict standard deviation. (B–D) Annexin V/DAPI data expressed in terms of absolute cell counts per condition at 24, 48, and 72 hours (respectively). Viable (green – Annexin V negative, DAPI negative), early apoptosis (orange – Annexin V positive, DAPI negative), late apoptosis (blue – Annexin V positive, DAPI positive), dead (black – Annexin V negative, DAPI positive). n = 1.

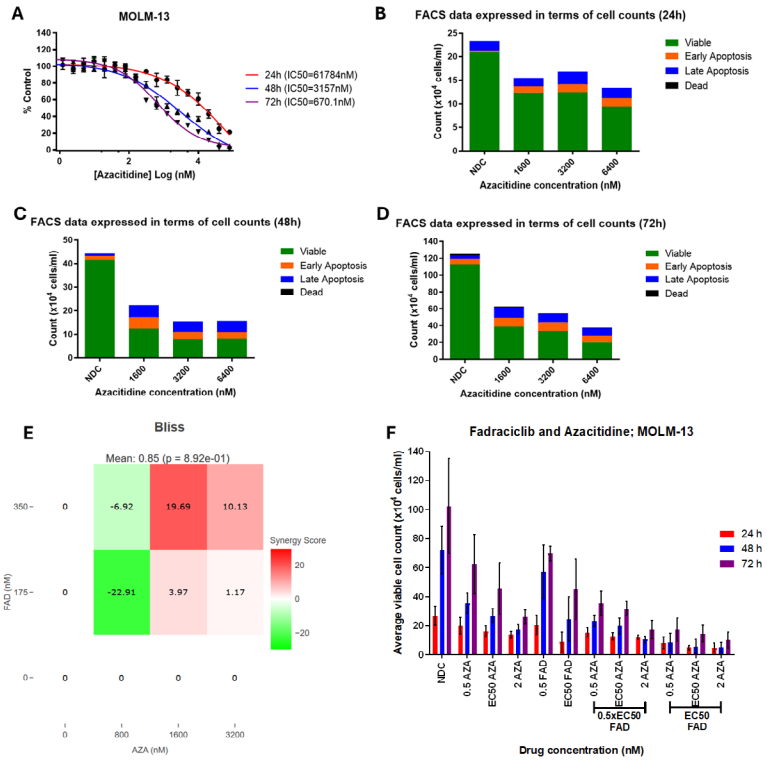

Figure S7. Determining the EC50 of azacitidine (AZA) on MOLM-13 cells and the optimal combination with fadraciclib. The concentrations used were 1,600 nM, 3,200 nM, and 6,400 nM (0.5× EC50, EC50, and 2× EC50 from the 48-hour resazurin assay). (A) Logarithmic graph showing the results of the resazurin assays (n = 3) at 24 (red), 48 (blue), and 72 hours (purple). (B–D) Annexin V/DAPI data expressed in terms of absolute cell counts per condition at 24, 48, and 72 hours (respectively). (E) Heatmap displaying the synergy calculated for each dosage combination using the Bliss Independence model at 48 hours. Heatmap produced using Synergy Finder+ software. (F) A bar chart depicting all fadraciclib and azacitidine combinations assessed on MOLM-13 cells. The cell numbers were calculated using trypan blue staining, and the proportion of viable cells was taken from Annexin V/DAPI staining. FAD EC50: 350 nM, AZA EC50: 1,600 nM. 24 h: Red, 48 h: blue, 72 h: purple. Bars represent the average of three biological replicates, with standard deviation depicted as error bars.

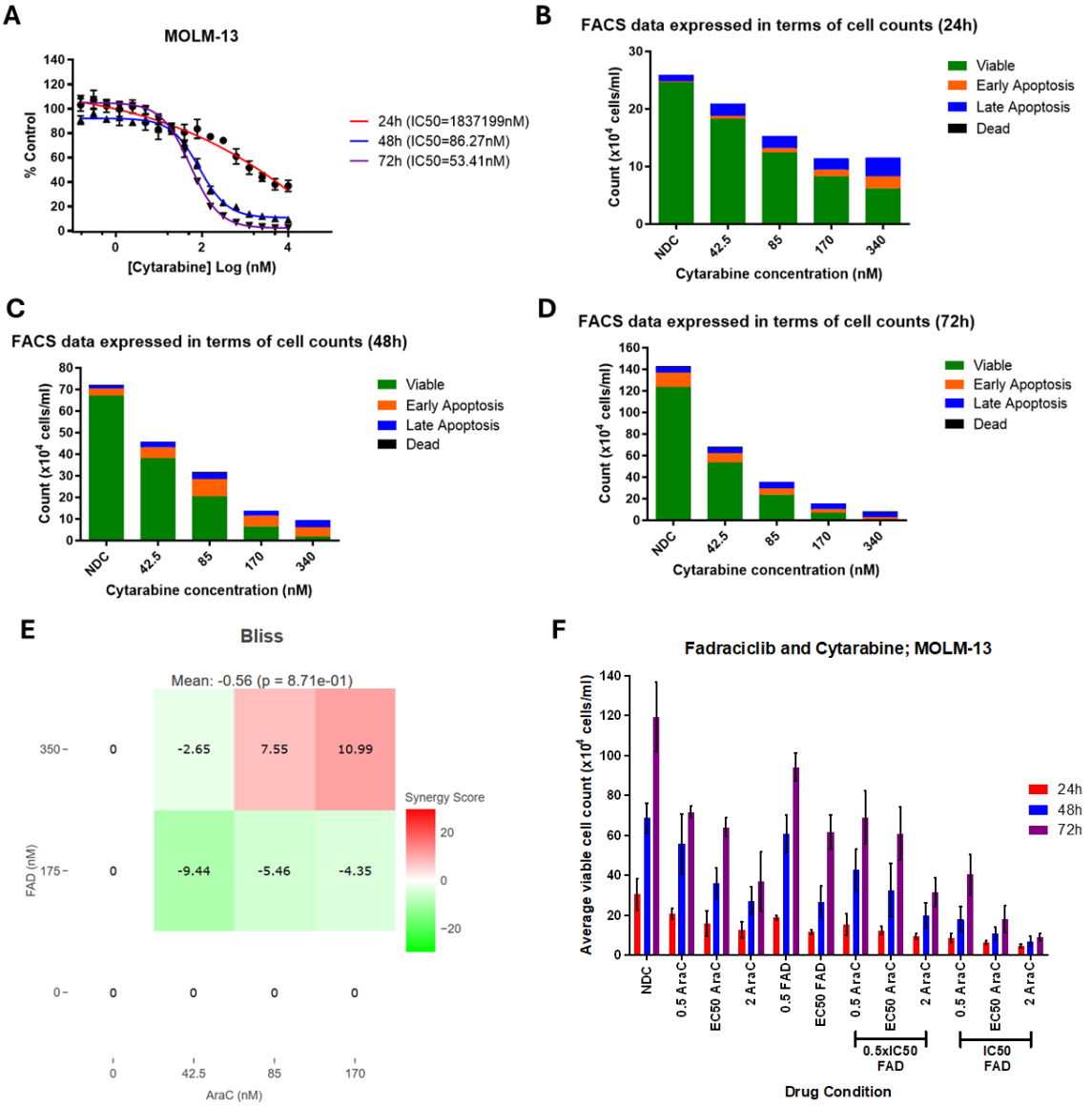

Figure S8. Determining the EC50 of cytarabine (AraC) on MOLM-13 cells and dose optimisation with fadraciclib. (A) Logarithmic graph displaying the results of the resazurin assays ($n = 3$) at 24 (red), 48 (blue), and 72 hours (purple). (B–D) Annexin V/DAPI data expressed in terms of absolute cell counts per condition at 24, 48, and 72 hours (respectively). The cells were treated with 42.5 nM, 85 nM, 170 nM, and 340 nM (0.5× EC50, EC50, 2× EC50, and 4× EC50 from the 48-hour resazurin assay). (E) Heatmap displaying the synergy calculated for each dosage combination using the Bliss Independence model at 48 hours. Heatmap produced using Synergy Finder+ software. (F) A bar chart depicting all fadraciclib and cytarabine combinations assessed on MOLM-13 cells. The cell numbers were calculated using trypan blue staining, and the proportion of viable cells was taken from Annexin V/DAPI staining. FAD EC50: 350 nM, AraC EC50: 42.5 nM. 24 h: Red, 48 h: blue, 72 h: purple. Bars represent the average of three biological replicates, with standard deviation depicted as error bars.

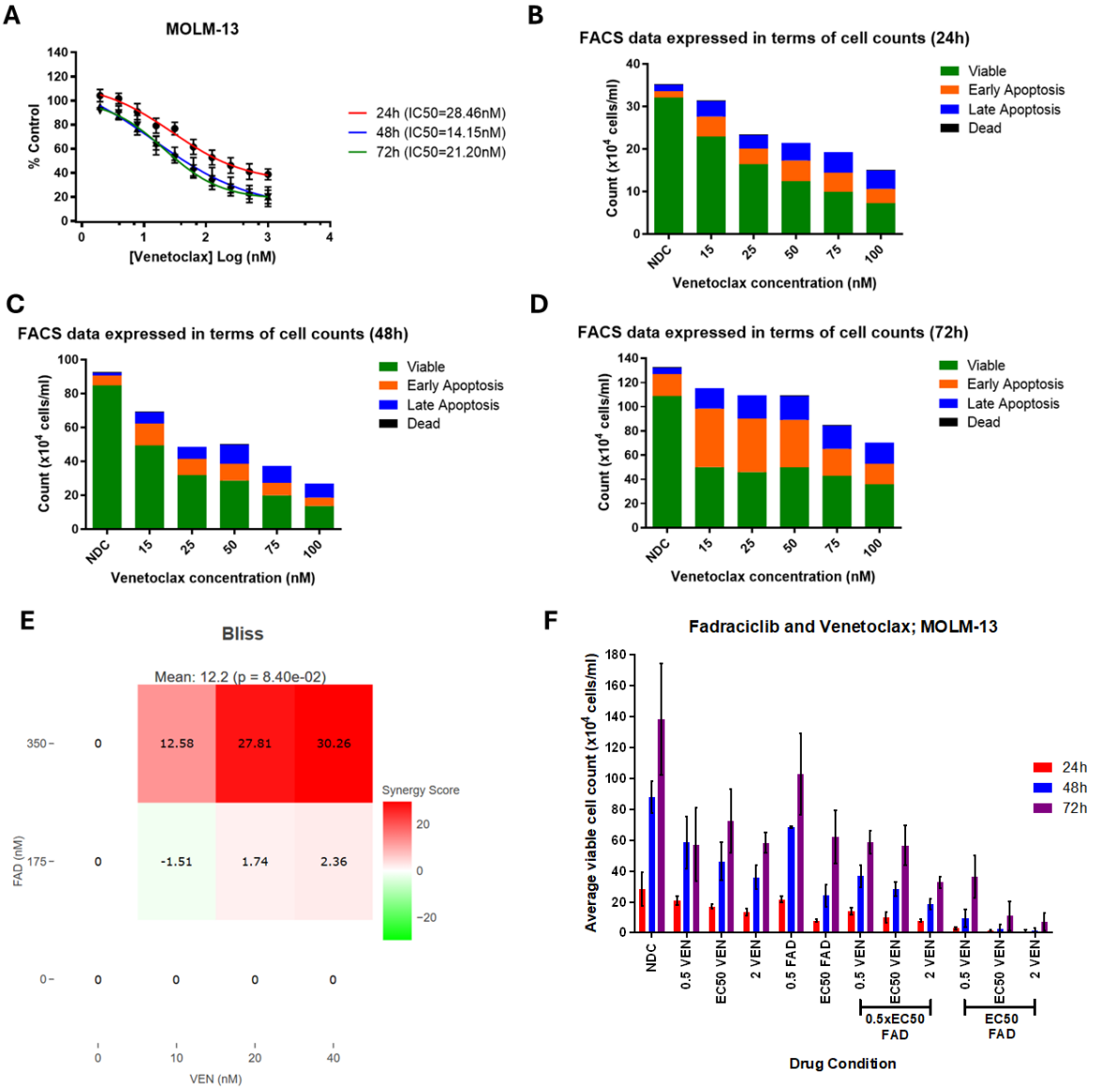

Figure S9. Determining the EC50 of venetoclax (VEN) and the optimal combination of venetoclax and fadraciclib on MOLM-13 cells. A: Logarithmic graph displaying the results of the resazurin reduction assays ($n = 3$) at 24 (red), 48 (blue), and 72 hours (purple). (B–D) Annexin V/DAPI data expressed as absolute cell counts per condition at 24, 48, and 72 hours (respectively). (E) Heatmap displaying the synergy calculated for each dosage combination using the Bliss Independence model at 48 hours. Heatmap produced using Synergy Finder+ software. (F) A bar chart depicting all fadraciclib and venetoclax combinations assessed on MOLM-13 cells. The cell numbers were calculated using trypan blue staining, and the proportion of viable cells was taken from Annexin V/DAPI staining. Due to the potency of these combinations, the 0.5× EC50 values of fadraciclib and venetoclax were selected (FAD 0.5× EC50: 175 nM, VEN 0.5× EC50: 10 nM). 24 h: red, 48 h: blue, 72 h: purple. Bars represent the average of three biological replicates, with standard deviation depicted as error bars.

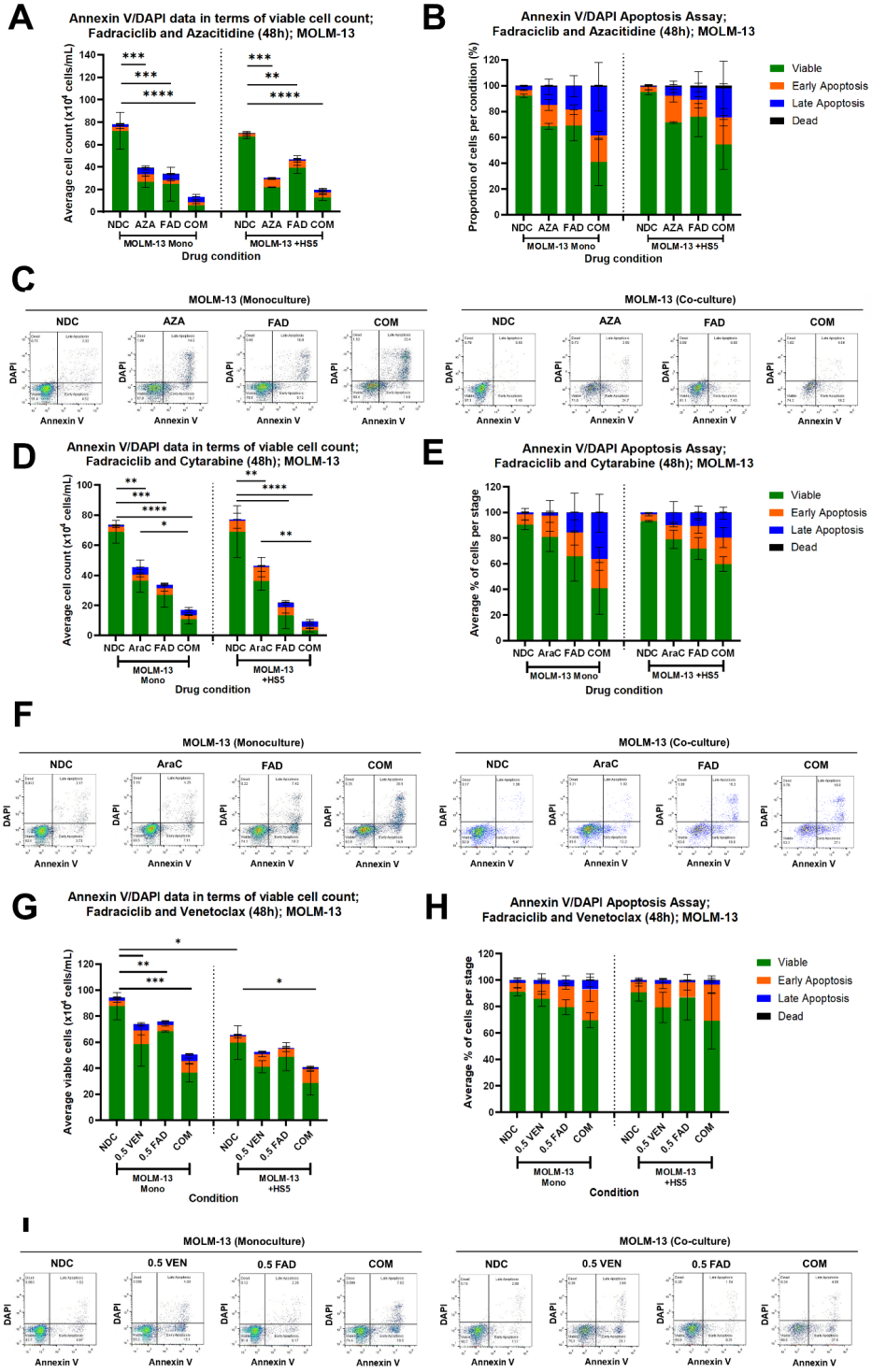

Figure S10. MOLM-13 cells in 2D monoculture and HS5 co-culture treated with fadraciclib and current AML therapies. (A, D, G) Annexin V/DAPI data shown in terms of cell counts for MOLM-13 cells treated with fadraciclib (FAD) alone, in combination with azacitidine (AZA; A), cytarabine (AraC; D) or venetoclax (VEN; G) and combination (COM) therapy in monoculture and co-culture. (B, E, H) Bar chart showing the proportion of cells in each apoptotic stage through Annexin V/DAPI apoptosis staining for FAD alone and in combination with AZA (B), AraC (E), or VEN (H). A one-way ANOVA was used to detect significant differences between conditions in (B), (E), and (H). (C, F, I) Representative Annexin V/DAPI scatter plots showing the proportions of NDC and drug-treated MOLM-13 cells in monoculture (left) and co-culture (right) in each stage of apoptosis 48 hours post-treatment. Significance: * $p \leq 0.05$; ** $p \leq 0.01$; *** $p \leq 0.001$, **** $p \leq 0.0001$. Bars represent the mean of three biological replicates, and standard deviation is depicted as error bars.

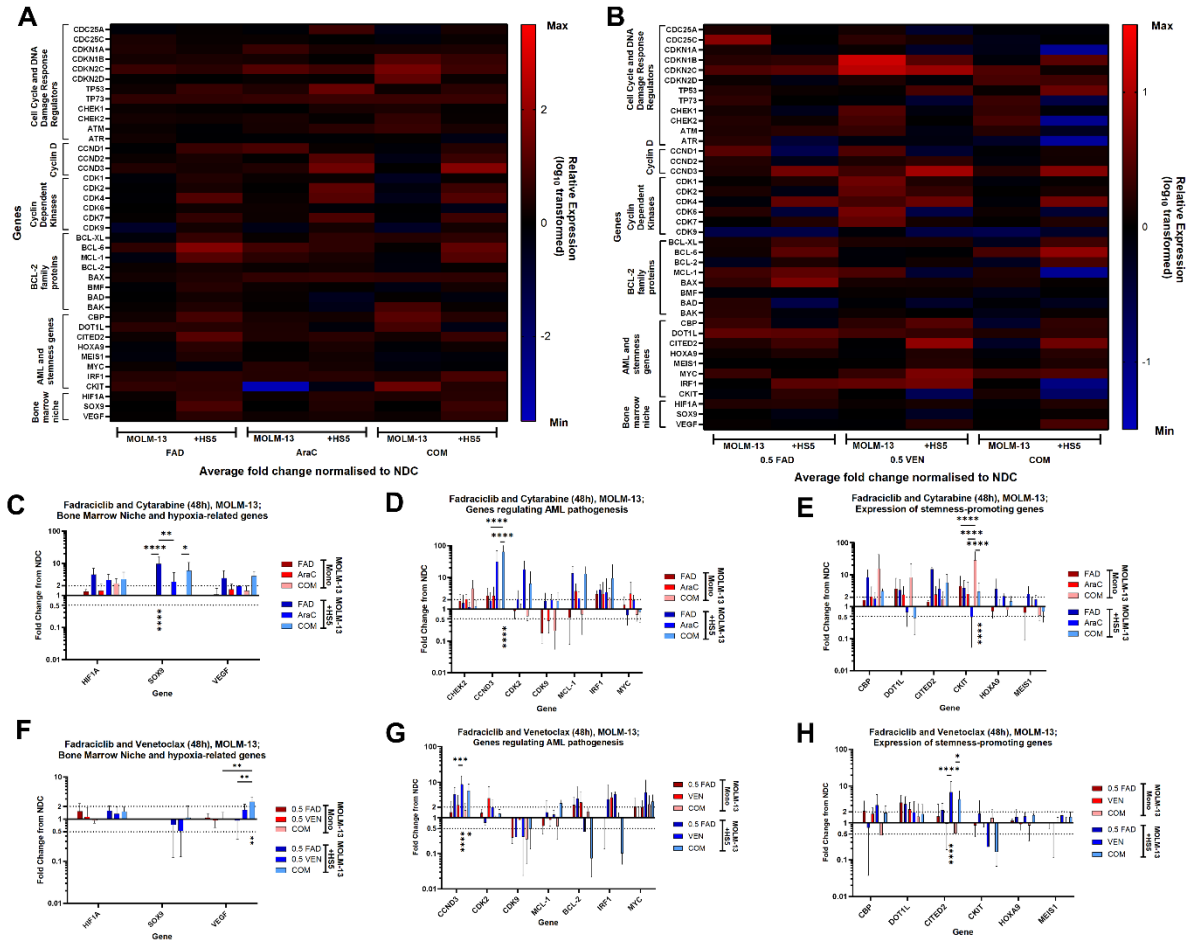

Figure S11. The effect of fadraciclib alone and in combination with cytarabine and venetoclax on MOLM-13 gene expression. (A, B) Heat maps displaying differences in gene expression for MOLM-13 cells in monoculture and HS5 co-culture following treatment with fadraciclib (FAD) alone and in combination with cytarabine (AraC, A) or venetoclax (VEN, B), normalised to NDC. Blue: downregulated compared to NDC; red: upregulated. (C, F) Bone marrow niche and hypoxia-related gene expression after treatment with cytarabine (C) and venetoclax (F); (D, G) expression of genes regulating AML pathogenesis after cytarabine (D) and venetoclax (G) treatments; (E, H) stemness-promoting gene expression after cytarabine (E) and venetoclax (H) single and combination treatments. Two-way ANOVAs with multiple comparisons were used to detect significant differences between conditions in the bar-chart panels (C–H). Significance: * $p \leq 0.05$; ** $p \leq 0.01$; *** $p \leq 0.001$, **** $p \leq 0.0001$. Bars represent the mean of three biological replicates, and standard deviation is depicted as error bars.

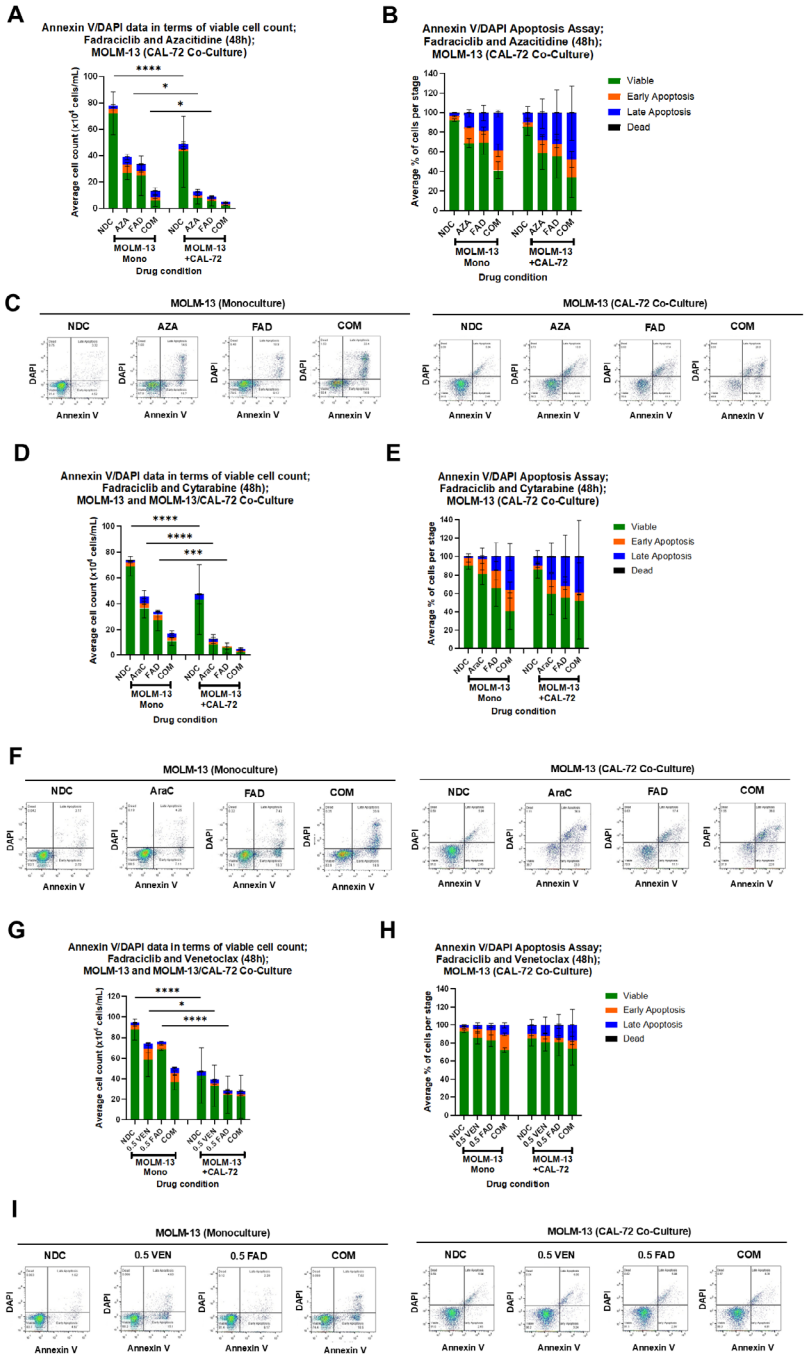

Figure S12. MOLM-13 cells in 2D monoculture and CAL-72 co-culture treated with fadraciclib and selected AML therapies. (A, D, G) Annexin V/DAPI data shown in terms of cell counts for MOLM-13 cells treated with fadraciclib (FAD), azacitidine (AZA; A), cytarabine (AraC; D) or venetoclax (VEN; G) and combination (COM) therapies of fadraciclib with these drugs in monoculture and CAL-72 co-culture. (B, E, H) Bar chart showing the proportion of cells in each apoptotic stage through Annexin V/DAPI apoptosis staining for FAD alone and in combination with AZA (B), AraC (E), or VEN (H) in monoculture and CAL-72 co-culture. A one-way ANOVA was used to detect significant differences between conditions in (B), (E), and (H). (C, F, I) Representative Annexin V/DAPI scatter plots showing the proportions of NDC and drug-treated MOLM-13 cells in monoculture (left) and CAL-72 co-culture (right) in each stage of apoptosis. Significance: * $p \leq 0.05$; ** $p \leq 0.01$; *** $p \leq 0.001$, **** $p \leq 0.0001$. Bars represent the mean of three biological replicates, and standard deviation is depicted as error bars.

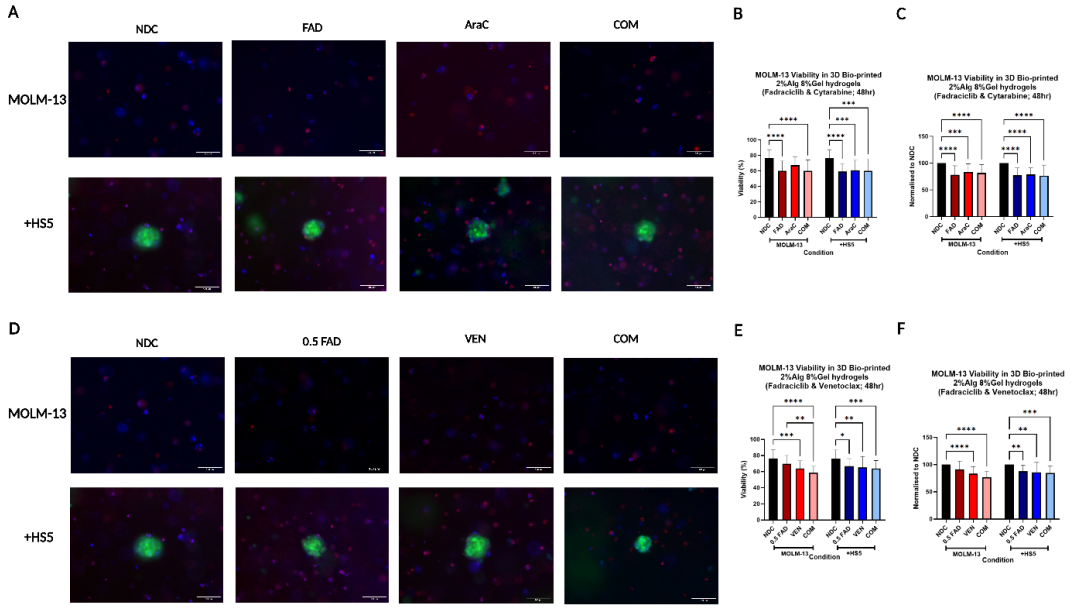

Figure S13. MOLM-13 cells in 3D monoculture and HS5 spheroid co-culture treated with fadraciclib with cytarabine or venetoclax. (A, D) Representative images of 3D-bioprinted MOLM-13 cells in monoculture and HS5 spheroid co-culture 48 hours after treatment with fadraciclib (FAD), cytarabine (AraC), venetoclax (VEN) or a combination of FAD with AraC or VEN (COM). Images taken at 20× using the M7000 Imager (scale bar: 100 µm). Green: HS5 cells (GFP-HS5 cells); blue: live cells; red: dead cells. (B, E) MOLM-13 cell viability within 3D-bioprinted 2%Alg8%Gel hydrogels following drug treatment. (C, F) MOLM-13 cell viability normalised to NDC. One-way ANOVAs with multiple comparisons were used to find significant differences between conditions in (B), (C), (E), and (F). Significance: * $p \leq 0.05$; ** $p \leq 0.01$; *** $p \leq 0.001$, **** $p \leq 0.0001$. Bars represent the mean of three biological replicates, and standard deviation is depicted as error bars.

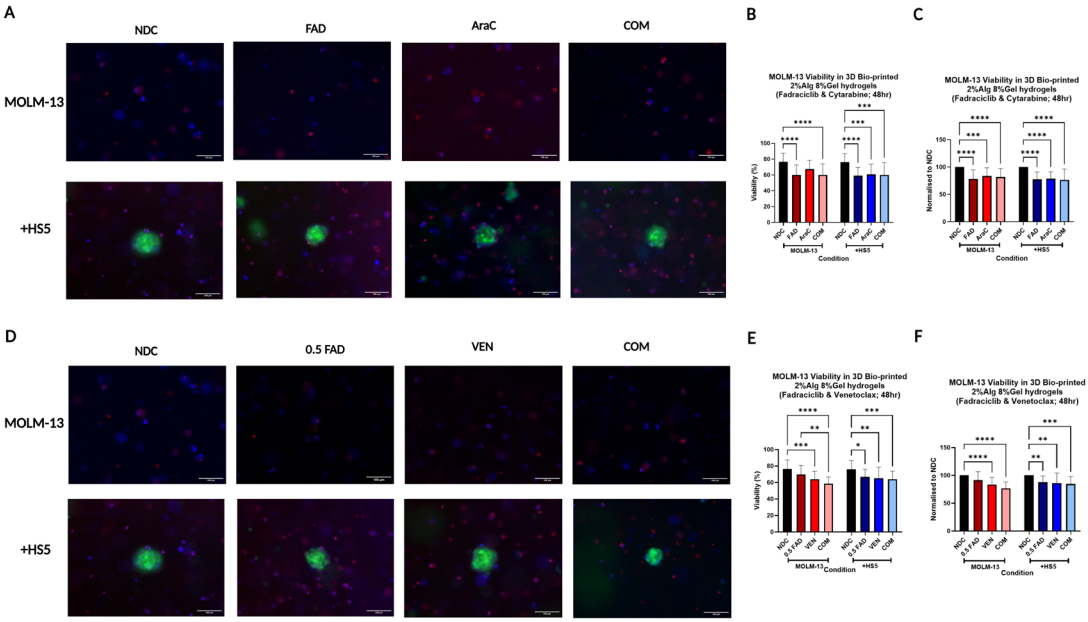

Figure S14. Assessment of fadraciclib with cytarabine or venetoclax within the final 3D-bioprinted model. (A, D) Representative images of the final 3D-bioprinted AML model, comprising MOLM-13 cells in monoculture and HS5 spheroid co-culture cultured with a CAL-72 monolayer. Images taken 48 hours after treatment with fadraciclib (FAD), cytarabine (AraC), venetoclax (VEN) or a combination of FAD with AraC or VEN (COM). Images taken at 20× using the M7000 Imager (scale bar: 100 µm). Green: HS5 cells (GFP-HS5 cells); blue: live cells; red: dead cells. (B, E) MOLM-13 cell viability within 3D-bioprinted 2%Alg8%Gel hydrogels following drug treatment. (C, F) MOLM-13 cell viability normalised to NDC. One-way ANOVAs with multiple comparisons were used to find significant differences between conditions in (B), (C), (E), and (F). Significance: * $p \leq 0.05$; ** $p \leq 0.01$; *** $p \leq 0.001$, **** $p \leq 0.0001$. Bars represent the mean of three biological replicates, and standard deviation is depicted as error bars.

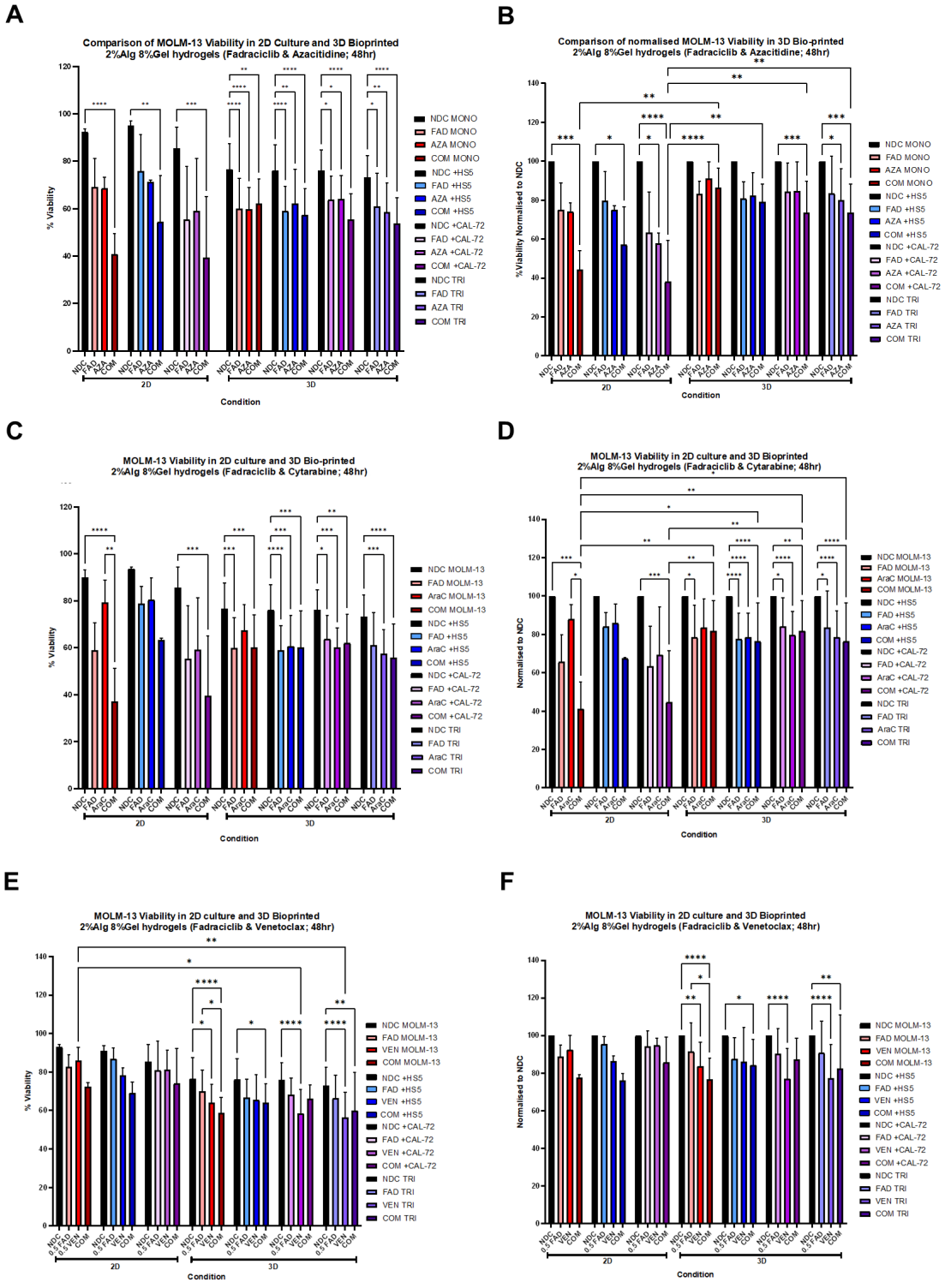

Figure S15. Bar charts comparing all conditions assessed within this study for fadraciclib in combination with azacitidine, cytarabine and venetoclax. (A, C, E) MOLM-13 viability after treatment with fadraciclib (FAD), azacitidine (AZA; A), cytarabine (AraC, C) and venetoclax (VEN, E) in all 2D and 3D conditions. (B, D, F) MOLM-13 cell viability normalised to NDC following treatment with FAD and AZA (B), AraC (D) and VEN (F). One-way ANOVAs with multiple comparisons were used to detect significant differences between conditions. Significance: * $p \leq 0.05$; ** $p \leq 0.01$; *** $p \leq 0.001$, **** $p \leq 0.0001$. Bars represent the average of three biological replicates, with standard deviation shown as error bars.

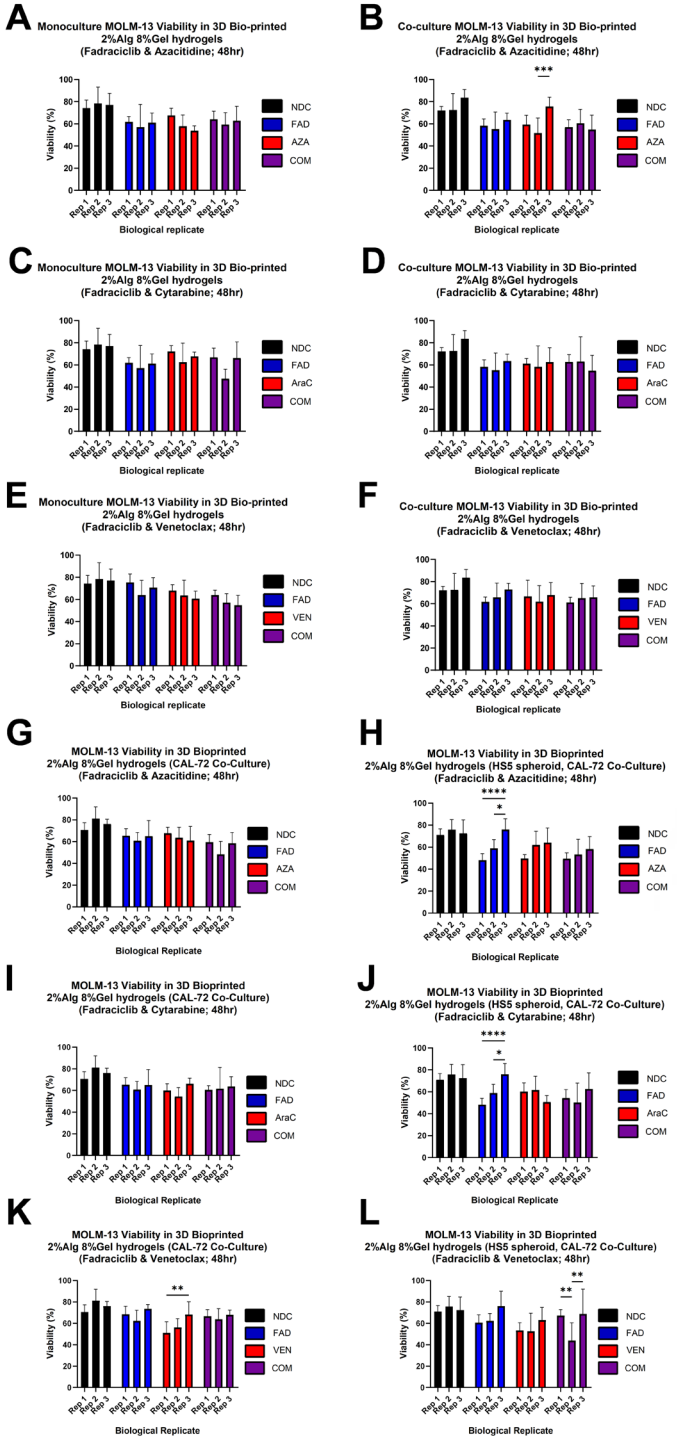

Figure S16. Assessing inter-replicate variability in 3D-bioprinted MOLM-13 cells treated with selected chemotherapies. Each biological replicate was compared to the other biological replicates (n = 9 technical replicates each) to assess whether the results obtained from the intermediate 3D model (A–F, no CAL-72 monolayer) and the final 3D model (G–L, with CAL-72 monolayer) were reproducible across experiments. One-way ANOVAs with multiple comparisons were completed to detect significant differences. Overall, few significant differences were found between replicates, highlighting that this model is highly reproducible. Significance: * $p \leq 0.05$; ** $p \leq 0.01$; *** $p \leq 0.001$, **** $p \leq 0.0001$. Bars represent the mean of three biological replicates, and standard deviation is depicted as error bars.

Notes: Rep: replicate. FAD: fadraciclib. AZA: azacitidine. AraC: cytarabine. VEN: venetoclax. COM: combination therapy of fadraciclib plus the additional selected chemotherapy in each graph.

Table S1. Summary of estimated half-maximal effective/inhibitory concentrations (nM) for MOLM-13 cells

Drug	24 hours	48 hours	72 hours
Fadraciclib	350	350	350
Azacitidine	6,400	1,600	1,600
Cytarabine	85	85	42.5
Venetoclax	25	20	15

Notes: These concentration ranges were estimated using resazurin assays and determined using Annexin V/DAPI staining and trypan blue exclusion staining. Concentrations are measured in nM.

Table S2. Primers selected for multiplex qRT-PCR

Primer	Gene	Forward (5' to 3')	Reverse (5' to 3')
ATM	Ataxia-telangiectasia mutated	CGGAGCTGATTGTAGCAACATACTA	CAGATAGAGCCTGAAGTACACAGAG
ATP5B	ATP synthase F1 subunit beta	TCCATCCTGTCAGGGACTATG	ATCAAACTGGACGTCCACCAC
ATR	Ataxia telangiectasia and Rad3-related	CAGCTCTCTATGAAGGCCATTCAA	GTTCTACTGTTTCACTGTCTGTTGC
B2M	Beta-2 microglobulin	GTCTTTCAGCAAGCACTGGTCT	CTTAGATGTCTCGATCCCACTT
BAD	BCL2-associated agonist of cell death	CTTTAAGAAGGGACTTCCTCGCC	CAAGTTCCGATCCCACCAGG
BAK	BCL2 antagonist/killer 1	TCATCGGGGACGACATCAAC	CAAACAGGCTGGTGGCAATC
BAX	BCL2-associated X protein	GACATTGGACTTCCTCCGGG	ACAGGGACATCAGTCGCTTC
BCL2	B-cell CLL/lymphoma 2	CCCTGTGGATGACTGAGTACC	GTTCCACAAAGGCATCCCAGC
BCL6	B-cell lymphoma 6	GCACTTGGGACCACAGAGAAA	ATGCCTTGCTTCACAGTCCA
BCLXL	B-cell lymphoma extra large	AGCTGGTTTTTTTGCCAGCC	TCTCTTCTAAGATCCAAAGCC
BMF	Bcl-2-modifying factor	GAACCCCAGCGACTCTTTTA	TTTCGGGCAATCTGTACCTC
CBP	CREB-binding protein	TTCTTCCCGGAGACTGAGGT	GACAGGGAGGATGGAGGAGT
CCND1	Cyclin D1	GATCAAGTGTGACCCGGACTG	CCTTGGGGTCCATGTTCTGC
CCND2	Cyclin D2	CACCAACACAGACGTGGATTG	CTCCGACTTGGATCCGTCAC
CCND3	Cyclin D3	CAGAGCCTGCTCCGCC	CTGCTCCTCACATACCTCCA
CDC25A	Cell division cycle 25A	GTCTAGATTCTCCTGGGCCATTG	CAGAATGGCTCCTCTTCAGAGC
CDC25B	Cell division cycle 25B	GTTTGTTGGCTGCCCTGC	CGACAGGGAGGATTCGGATG
CDC25C	Cell division cycle 25C	AATGTAGCCCAGCACAGCTT	GTAAGGCAGCCACCTTGGAA
CDK1	Cyclin-dependent kinase 1	ATGAAGTGTGGCCAGAAGTG	CAGAAATTCGTTTGGCTGGATCA
CDK2	Cyclin-dependent kinase 2	GCTTGTTATCGCAAATGCTGC	GATGGGGTACTGGCTTGGTC
CDK4	Cyclin-dependent kinase 4	GAAACTCTGAAGCCGACCAG	AGGCAGAGATTCGCTTGTGT
CDK6	Cyclin-dependent kinase 6	CCTGCAGGGAAAGAAAAGTGC	CCTCCTCTTCCCTCCTCGAA
CDK7	Cyclin-dependent kinase 7	GTGGCCGGACATGTGTAGTC	GCCGTAATTCGAGCACATGG
CDK9	Cyclin-dependent kinase 9	ATGGAAAACGAGAAGGAGGGG	TAGGGGGAAGCTTTGGTTCG

(*cont'd...*)

Table S2. (*Continued*)

Primer	Gene	Forward (5' to 3')	Reverse (5' to 3')
CDKN1A	Cyclin-dependent kinase inhibitor 1A	TCTTGTACCCTTGTGCCTCG	CGGCGTTTGGAGTGGTAGAA
CDKN1B	Cyclin-dependent kinase inhibitor 1B	GGCTAACTCTGAGGACACGC	TGAGTAGAAGAATCGTCGGTTGC
CDKN2C	Cyclin-dependent kinase inhibitor 2C	AGAAACTGTCACTGGGAGCG	AGGCTCGGCCATTCTTTAGG
CDKN2D	Cyclin-dependent kinase inhibitor 2D	GGCAGTTCAAGAGGGTCACA	GTCCCTGCGATGGAGATCAG
CHEK1	Checkpoint kinase 1	GGTCACAGGAGAGAAGGCAATA	GGAAGAATCTCTGAGCATCTGG
CHEK2	Checkpoint kinase 2	AGTGGATCCAAAGGCACGTT	CCTGGGGTAGAGCTGTGGAT
CITED2	Cbp/P300-interacting transactivator with Glu/Asp rich carboxy-terminal domain 2	GCGAGCACATACACTACGGC	CCATGAACTGGGAGTTGTTAAACC
CKIT	KIT proto-oncogene	GCATTCAAGCACAATGGCAC	CCAATCAGCAAAGGAGTGAA
DOT1L	Disruptor of telomeric silencing 1-like	CAGTGAGAAGGGCCTGAGAG	TGGAGTTGAGGTTGAGGGGA
ENOX2	Ecto-NOX disulfide-thiol exchanger 2	CACTGGCACTACCAAACTGCA	GAGCTGGAGGGAACCTGATTT
GUSB	Glucuronidase beta	GAGCAAGACAGTGGGCTGG	CCATTCGCCACGACTTTGTT
HIF1A	Hypoxia-inducible factor 1 subunit alpha	TACTCATCCATGTGACCATGAGG	TAGTTCTTCCTCGGCTAGTTAGG
HOXA9	Homeobox A9	CCCCATCGATCCCAATAACCC	TCCCTGGTGAGGTACATGTTG
IRF1	Interferon regulatory factor 1	ACCTCTGCCTTCTTCCCTCT	CATCCGAGTGATGGGCATGT
JUN	Jun proto-oncogene, AP-1 transcription factor subunit	GGGGTTGACTGGTAGCAGAT	CTGTGTCTGTCTGTCTGCCT
MCL1	Myeloid cell leukaemia 1	GCCTTCCAAGGATGGGTTTG	TATGCCAAACCAGCTCCTACTC
MEIS1	Meis homeobox 1	ATGGCGCAAAGGTACGACG	TACTGATGCGAGTGCAGAGG
MYC	MYC proto-oncogene, bHLH transcription factor	GACTCTGAGGAGGAACAAGA	TCGTCGCAGTAGAAATACGG
TP53	Tumour protein p53	TGTGACTTGCACGTACTCCC	TCCGTCATGTGCTGTGACTG
SOX9	SRY-box transcription factor 9	ATCTCCCCCAACGCCATCTT	CTGGGATTGCCCCGAGTG
TBP	TATA-box binding protein	ATCTTTGCAGTGACCCAGCAT	CTTGCGCTGGAACTCGTCT
TP73	Tumour protein p73	ACTTTGAGATCCTGATGAAGC	GAGGACCGGCCCGTAGGA
TYW1	TRNA-YW synthesizing protein 1 homolog	CTCCTGATAGCACACAGAAAGTTTA	TGCGCTGAACGTTTTTGATCC
VEGF	Vascular endothelial growth factor	AGAAGGAGGAGGGCAGAATCA	AGGGTACTCCTGGAAGATGTCC